A strontium lattice clock with 3×10^{-17} inaccuracy and its frequency

A strontium lattice clock with 3×10^{-17} inaccuracy and its frequency

Stephan Falke, Nathan Lemke, Christian Grebing, Burghard Lipphardt, Stefan Weyers, Vladislav Gerginov, Nils Huntemann, Christian Hagemann, Ali Al-Masoudi, Sebastian Häfner, Stefan Vogt, Uwe Sterr and Christian Lisdat

Physikalisch-Technische Bundesanstalt (PTB), Bundesallee 100, D-38116 Braunschweig; Germany
E-mail: christian.lisdat@ptb.de

Abstract

We have measured the absolute frequency of the optical lattice clock based on ^{87}Sr at PTB with an uncertainty of 3.9×10^{-16} using two caesium fountain clocks. This is close to the accuracy of today's best realizations of the SI second. The absolute frequency of the $5s^2$ $^1S_0$ – $5s5p$ $^3P_0$ transition in ^{87}Sr is 429 228 004 229 873.13(17) Hz. Our result is in excellent agreement with recent measurements performed in different laboratories worldwide. We improved the total systematic uncertainty of our Sr frequency standard by a factor of five and reach 3×10^{-17}, opening new prospects for frequency ratio measurements between optical clocks for fundamental research, geodesy or optical clock evaluation.

Keywords: optical lattice clock, SI second, relativistic geodesy

1. Introduction

Motivated by the prospect for a redefinition of the SI second based on an optical transition, optical clocks employing various atomic species and reference transitions are currently being developed and refined worldwide [1–6]. Although optical clocks achieve accuracies and

stabilities superior to primary standards, only two frequency measurements limited by today's most accurate realization of the SI second have been reported so far [7, 8]. Such measurements are essential prerequisites for a possible redefinition of the second. Here, we present a third that is in very good agreement with the measurement in Paris [7]. In addition to their role as future primary standards, optical clocks are of interest as sensitive probes in areas such as relativistic geodesy [9], tests of relativity [10, 11], and searches for variations of fundamental constants [1, 12–15].

Two types of optical clocks have emerged: single ion clocks and optical lattice clocks. While in ion clocks a single reference atom is trapped utilizing its electric charge, in optical lattice clocks thousands of neutral atoms are trapped in an optical potential that is carefully tuned to the AC-Stark-shift-cancelling (magic) wavelength [16]. Several ion clock systems have demonstrated very low systematic uncertainties on the order of 10^{-17} [1, 4, 5, 17]. While the frequency stability of optical lattice clocks is superior [18, 19], their systematic uncertainty had been limited to approximately 10^{-16} [3, 7, 20, 21]. However, a recent study placed strontium lattice clocks into the accuracy regime of the best ion clocks [22].

The leading uncertainty contribution in lattice clocks is typically from the blackbody radiation (BBR) Stark shift [23, 24]. For the cases of Sr and Yb, recent measurements and calculations of the relevant atomic polarizabilities [25–28, 38] have mitigated this key source of error, enabling lattice clocks to push the total systematic uncertainty below 10^{-16} for the first time. Simultaneously, several groups have reduced the noise of the interrogation oscillators [29, 30], which has in turn led to significantly reduced clock instabilities [18, 19, 31]; this improved instability then allows for a very rapid and thorough investigation of systematic effects.

The accuracy of today's best Cs fountain clocks of 2–4×10^{-16} [32–36] sets a limit for the achievable accuracy of frequency measurements. For a measurement at this level the optical standard needs to be sufficiently accurate as well as operationally robust in order to accommodate the long averaging times required by the microwave standard. Moreover, the link between the optical and microwave standards must be carefully controlled to avoid possible errors. In this paper we report a frequency measurement of the clock transition $5s^2\,{}^1S_0\,$–$\,5s5p\,{}^3P_0$ in ^{87}Sr against two caesium fountain clocks at PTB with a total uncertainty of 3.9×10^{-16}. The systematic uncertainty of the strontium clock is below that of the caesium fountains by nearly one order of magnitude, benefiting from the much higher operating frequency of 429 THz compared to 9.2 GHz. This evaluation of a lattice clock accuracy is among the best [22] and indicates that the quest for the most accurate clock is open to atoms and ions.

The paper is organized as follows: first, we describe our strontium lattice clock setup. In section 3 we report on the study of systematic frequency shifts and obtain the uncertainty budget. This is followed in section 4 by a description of the absolute frequency measurement. Finally, we report and discuss our results in section 5.

2. Strontium lattice clock setup

The preparation of ultracold ^{87}Sr atoms (nuclear spin $I = 9/2$) in an optical lattice follows commonly applied procedures. Here we give a general overview of the setup and refer to previous publications [21, 37, 38] for details. A level scheme reduced to the relevant levels and transitions is shown in figure 1. The atom source is an oven operated at 770 K with no direct
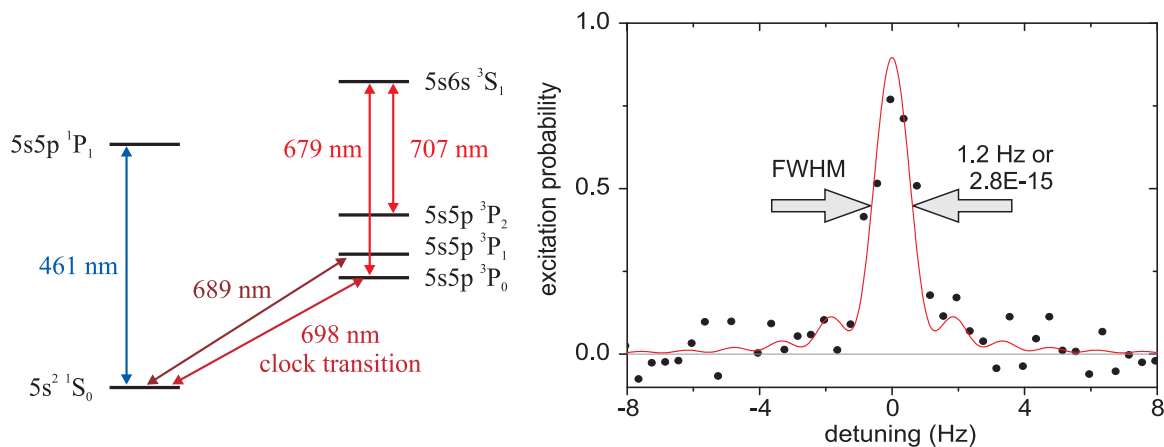
Figure 1. Simplified level scheme of strontium with arrows indicating the required cooling and spectroscopy lasers and their wavelengths (left) and scan across the clock transition (right). The observed data (dots, single recording per point) are accompanied by a simulated spectrum (line) obtained by a numerical evaluation of the density matrix with a clock laser of linewidth of 0.08 Hz. The clock pulse length is 720 ms in both experiment and simulation. Due to noise and background subtraction, unphysical negative probabilities appear.

line of sight between the atom source and the magneto-optical trap (MOT). Atoms are Zeeman-slowed and captured in a MOT operated near the strong singlet transition $^1S_0 - ^1P_1$ at 461 nm to obtain samples at a few millikelvin. Originally an optical molasses had been applied to guide the slowed atoms into the MOT region [37] but it was deemed not necessary for efficient loading and is not present in this work. A second stage MOT operated on the $^1S_0 - ^3P_1$ transition at 689 nm cools the sample to about $2\,\mu$K. Here, two frequencies are applied to avoid population trapping by connecting the $^1S_0$ state to the $F = 9/2$ and $F = 11/2$ states of $^3P_1$ [39]. Initially, this MOT uses high laser intensity and a laser frequency modulation to ensure an efficient transfer from the first-stage MOT. Subsequently, at lower intensity and without frequency modulation, the atoms are cooled further and captured by a red-detuned optical lattice operating at $\lambda \approx 813$ nm, the magic wavelength [16] of the clock transition. The depth of the optical lattice is typically $k_B \times 14\,\mu$K or $80\,E_{rec}$, where $E_{rec} = h^2/(2\,m\lambda^2)$ is the recoil energy from a lattice photon, k_B is the Boltzmann constant, m is the mass of the atom and h is the Planck constant. The horizontally-oriented lattice is formed by retro-reflection of the ~300 mW output of a Ti:sapphire ring laser that is delivered to the position of the atoms via a large mode area (LMA) fibre to avoid Brillouin scattering at high power and focused to a waist radius ($1/e^2$ intensity) of $45\,\mu$m. A portion of the laser output is sent to a frequency comb in order to monitor and stabilize its frequency.

Once the second stage MOT is switched off, the lattice-trapped atoms are spin-polarized by optical pumping into one of the stretched levels $m_F = -9/2$ or $m_F = +9/2$. Then, the coldest atoms are selected by an energy filtering procedure wherein the optical lattice depth is ramped down within 5 ms to $28\,E_{rec}$ for 20 ms and only the atoms with energies below this barrier are kept. After ramping the depth back to $80\,E_{rec}$ in 5 ms, approximately 25% of the atoms remain in the trap. Here, we make use of an intensity control feedback loop acting on the diffraction efficiency of an acousto-optic modulator (AOM) between the laser and the LMA fibre. We servo the power of the retro-reflected light that travelled back through the LMA fibre
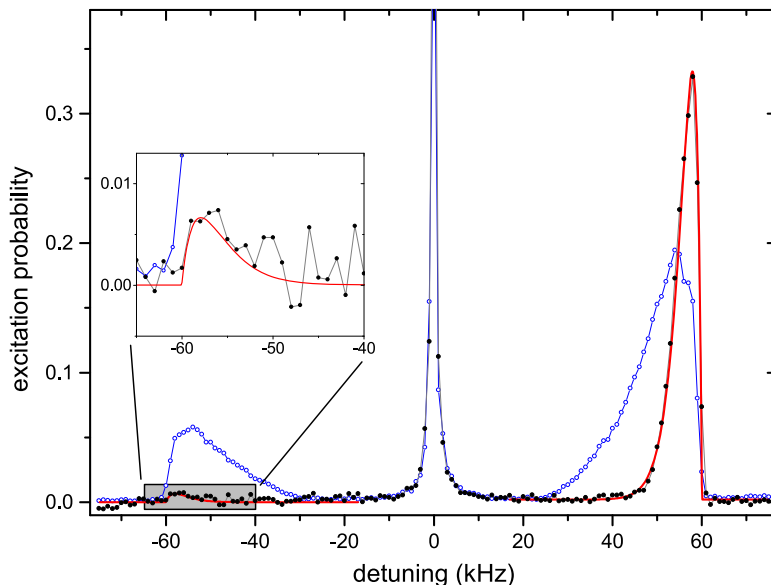
Figure 2. Sideband spectra before (blue open circles) and after (black points) the energy filtering procedure as described in the text. Along with the filtered experimental data a simulated line shape (red line) adjusted to the experimental data are shown. The inset shows an expanded view of the expected position of the red axial sideband. Here, the amplitude of the simulated spectrum was chosen to be 0.02 times the amplitude of the blue sideband. The filtering procedure reduces the average excitation in the axial and radial directions, as seen in the increased ratio of blue to red sideband intensity and reduced width of the sidebands, respectively.

as measured by a photodiode. The temperature of the ensemble is measured using sideband spectra (figure 2), which reveal an axial temperature $\lesssim 1\,\mu$K and a radial temperature of $2\,\mu$K after the filtering procedure. This analysis is based on the line shape model developed in [40]. The final temperature is insensitive to changes of the settings of several 10%. The reduced atomic kinetic energies after the filtering procedure are beneficial for reducing systematic effects (site-to-site tunnelling and lattice light shifts) as discussed below.

In order to combat impurities in the spin-polarization (i.e. residual population in the other m_F states), we apply a purification sequence as follows: first, a magnetic field of $625\,\mu$T is created utilizing the MOT coils in Helmholtz configuration. This field is sufficient to spectrally resolve the different m_F-components on the $\Delta m_F = 0$ clock transition (about 675 Hz between neighbouring components). We apply a short clock laser pulse and observe a line width of 23 Hz of the individual components, which is the Fourier width of the 35 ms π-pulse. The clock laser beam is linearly polarized parallel to the applied magnetic field. Atoms remaining in the ground state are driven out of the lattice using ${}^1S_0 - {}^1P_1$ resonant light. Depending on the initial spin-polarization and the laser detuning the atoms are prepared in either the $m_F = +9/2$ or the $m_F = -9/2$ substate of ${}^3P_0$.

The clock laser system at 698 nm is an extended cavity diode laser with an injection locked laser diode for power amplification. It is locked to a highly stable external resonator made from ULE (ultra low expansion glass). The frequency instability of the laser is further reduced by phase locking via a femtosecond comb to a $1.5\,\mu$m fibre laser stabilized to a single-crystal

silicon cavity [31] [1]. The optical path lengths to frequency comb and optical lattice are actively stabilized utilizing AOMs [41]. With this system, the short-term laser stability allows for interrogation times of 320 ms without loss of spectral contrast with a Fourier limited transition line width of 2.5 Hz (full width at half maximum). For this measurement, the magnetic field is reduced to about $25\,\mu$T. The AOM used for pulsing sets the required intensities, both for preparation and interrogation pulses. This interrogation de-excites atoms from the $^3P_0$ state to the $^1S_0$ ground state on a π-transition. Even narrower lines are observed as shown in figure 1 but for experimental robustness we operated the stabilization with 2.5 Hz linewidth.

The average transition probability of the ensemble of about 1500 atoms is then detected destructively by collecting laser induced fluorescence from the 461 nm transition on a photomultiplier tube. A first pulse measures the population in the $^1S_0$ state. Next, the atoms remaining in the $^3P_0$ state are optically pumped to the $^1S_0$ state using two repump lasers, after which a second detection of the $^1S_0$ atoms reveals the number of atoms that did not make the clock transition. Finally, the background signal is measured with a third pulse, completing the experimental cycle[2].

To realize a frequency standard, the clock laser is locked to the average frequency of the two $|m_F| = 9/2$ components removing the linear Zeeman effect. To derive an error signal, four interrogations at the transition half-width points are performed: two for $m_F = -9/2$ and two for $m_F = +9/2$. The addressing of the four points is done by frequency offsets on the AOM for pulsing the clock laser light. Hence the laser frequency as seen by the frequency comb is unaffected by this addressing.

3. Systematic frequency shifts

There are a number of possible frequency shifts of the clock transition that must be considered when characterizing a lattice clock's accuracy. The most significant are the BBR shift and lattice light shifts. We will discuss these in detail while keeping the discussion of other effects brief. A summary of the uncertainty contributions is given in table 1.

3.1. BBR shift

The largest frequency correction and residual uncertainty is due to the differential Stark shift of the clock states from BBR emitted by the apparatus surrounding the atoms. In an earlier work we have reported the BBR shift as a function of the environmental temperature [38] T in first-order approximation scaling with T^4. The determination of this temperature is discussed here. Assuming that the BBR seen by the atoms is that of an opaque system, this task is reduced to finding the representative temperature of the system. The assumption is justified as the windows of the vacuum system are not transparent for room temperature BBR. The oven is an external heat source and will be treated separately below. Even without any knowledge of the emissivity of the materials or detailed knowledge of the temperature distribution, it is clear that the representative temperature will be between that of the hottest and the coldest point of the closed system. We therefore identified the points of extreme temperatures on our vacuum chamber and

---

[1] This frequency comb is also part of the system counting the frequency of the clock laser.
[2] In the fluorescence detection, we have replaced a photodiode used previously by a photomultiplier (Hamamatsu H11526-110-NF) for noise reduction.

Table 1. Corrections and uncertainties of the strontium frequency standard during the frequency measurement given in fractional frequencies.

Effect	Correction $\left(10^{-17}\right)$	Uncertainty $\left(10^{-17}\right)$
BBR room	492.4	3.6
BBR oven	1.6	1.2
Second-order Zeeman	3.2	0.13
Cold collisions	0	0.5
Background gas collisions	0.15	0.15
Line pulling	0	0.03
Lattice scalar/tensor	0	0.9
Hyperpolarizability	−0.5	0.2
Lattice E2/M1	0	0.6
Tunnelling	0	0.1
Probe light	0	0.1
Optical path length error	0	0.08
Servo error	0	0.03
dc Stark shift	15.2	3.3
Total	512.0	5.2

monitored these temperatures with Pt-100 sensors, which have an uncertainty of 0.04 K near room temperature. We have verified the specified uncertainty by calibration of individual sensors and inter-comparison of all sensors before and after thermal and mechanical shock testing. To minimize the interval of the temperature, heat sources inside or close to the vacuum system must be avoided. The Zeeman slower is cooled with water whose temperature is controlled to within 0.1 K. A second closed cooling system controls the temperature of the MOT magnetic field coils made from copper tubing, which are located inside the vacuum chamber and are also used to create the bias magnetic field used during state preparation and clock interrogation. The thermal capacity of these coils averages the time-dependent heat load throughout the experimental cycle. We monitor the temperature of the inlet and outlet water with additional Pt-100 sensors. We have verified with a thermal camera viewing through a (usually blocked) zinc selenide viewport that the temperature gradient measured by these sensors corresponds to the width of the oberserved temperature range on the surface of the coils.

Once the minimal and maximal temperature T_{min} and T_{max} of the system are determined, a representative temperature and an associated uncertainty need to be derived. Without further knowledge or modelling of the thermal system, we assume a rectangular probability distribution for the representative temperature between T_{min} and T_{max}. Hence, according to BIPM's 'GUM: Guide to the Expression of Uncertainty in Measurement' [42], $T = \left(T_{min} + T_{max}\right)/2$ is the representative temperature with an uncertainty of $\left(T_{max} - T_{min}\right)/\sqrt{12}$, as this is the square root of the variance of the assumed probability distribution.

Compared to our previous frequency measurement [21], we improved the thermal homogeneity across the vacuum chamber by reducing the thermal loads. Specifically, magnetic field compensation coils are now externally mounted and water cooled. Moreover, the current in the Zeeman slower magnet is switched off when the slower is not in use. Typical temperatures

during operation have been $T_{min} = 293.71$ K and $T_{max} = 295.49$ K, and with the correction coefficients from [38] the shift correction is therefore $492.4\,(36) \times 10^{-17}$.

Despite these efforts, the uncertainty in the temperature is still a significant contribution to the uncertainty. One simple way to reduce this uncertainty is the inclusion of an additional time interval into the clock cycle, in which all magnetic coils are switched off. With an additional dead time of 1 s we have reached temperature intervals of $T_{max} - T_{min}$ of 1.2 K, corresponding to an uncertainty of 2.6×10^{-17} in studies following the absolute frequency measurement. This reduction of the heat load comes at the cost of the stability of the frequency standard, e.g. to $1.5 \times 10^{-15}\sqrt{s/\tau}$ for increasing the experimental cycle from 0.8 to 1.8 s.

The oven has no direct line of sight with the optical lattice but BBR photons emitted by the oven may be scattered towards the optical lattice. To consider the effect of these photons on the clock frequency, we apply a model that takes into account the temperature of the oven, a simplified geometry of the vacuum chamber, and the emissivity of the surface of the main vacuum chamber. For the uncertainty estimation of the oven induced BBR shift, uncertainties are applied to these parameters: the oven temperature is determined to $T_{oven} = 770\,(50)$ K. Three assumptions are made: first, we model the chamber geometry as a sphere with radius of 17 cm and the representative temperature T determined as described above. A small fraction of the sphere's surface, which corresponds to the size of the aperture between oven and Zeeman slower tube (circle of 2 mm diameter), is replaced by a surface that emits a different radiation spectrum. Second, we assume that this spectrum is a superposition of a BBR spectrum of the oven at T_{oven} transmitted through the Zeeman slower and the BBR spectrum of the slower itself at T. Without detailed modelling, a rectangular distribution between 0 and 1 is assumed for the transmission probability of oven BBR photons, leading to a scaling of the amplitudes of both spectra by 0.50(29). As a third assumption we use the model of [24] to describe the effect of multiply scattered oven-BBR photons using inside the spherical chamber an emissivity of polished stainless steel of 0.1 (with assumed minimal and maximal values of 0.07 and 0.2) [43]. The total effective shift due to scattered BBR photons emitted by the oven is -1.6×10^{-17}. Considering the uncertainties of the three discussed parameters, we obtain a combined uncertainty of 1.2×10^{-17}.

3.2. Optical lattice light shifts

A key concept of optical lattice clocks is to trap the atoms in a light field that, to first order in intensity, perturbs the two clock states equally. This is achieved by tuning the frequency of the laser light that creates the optical lattice to a magic wavelength; for Sr, the red-detuned magic wavelength is near 813 nm. Even at shallow trap depths, small effects due to higher order light shifts (both multipolar and two-photon) must be considered, as pointed out in [44]. We will account for these as discussed below, but first we describe the measurement of the magic wavelength.

For a particular lattice frequency, we compare the frequency of the clock transition with two different lattice intensities (80 E_{rec} and 160 E_{rec}) using an alternating stabilization method [37, 45]. The difference of the two offset frequencies between the atomic transition and the clock laser cavity mode is measured with independently working digital servo loops and gives the clock frequency dependence on the lattice intensity. The total Allan deviation [46] shown in figure 3 (blue markers) indicates the stability of this interleaved measurement as $\sigma_y(\tau) \approx 1.3 \times 10^{-15}(s/\tau)^{1/2}$. We expect that the instability of the clock operated with a single
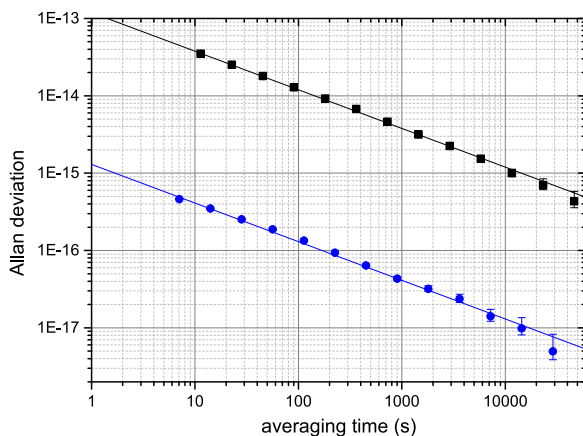
Figure 3. Instabilities of the frequency measurement. Shown are the Allan deviations of the comparison of the Yb$^+$ standard (black squares) and CSF2 and the total Allan deviation of an interleaved stabilization of the Sr frequency standard (blue circles). The estimated instability of the Sr frequency standard is a factor of two smaller than this observation. The lines indicate instabilities of 1.2×10^{-13} $(\mathrm{s}/\tau)^{1/2}$ and 1.3×10^{-15} $(\mathrm{s}/\tau)^{1/2}$.

stabilization instead of an interleaved one is at least a factor of two smaller. Although the atoms are very cold after the filtering procedure, their population distribution over the trap levels as observed in sideband spectroscopy needs to be considered when deriving the average lattice light intensity seen by the atoms [40]. We then correct the observed frequency difference for a difference in the quadratic light shift (hyperpolarizability) according to [44] using the coefficient given in [7] and the averaged intensity. This measurement and analysis is repeated at nine lattice frequencies in order to identify where the shift crosses zero. We derive the first order Stark-shift cancelling wavelength for $m_F = \pm 9/2$ with a linear regression of the corrected frequency differences normalized to the average light intensity experienced by the atom due to thermal motion and find 368 554 465.0 MHz.

In the measurement of the first order Stark-shift cancelling wavelength, uncertainties due to the hyperpolarizability, residual tunnelling, and collisions (discussed below) are added in quadrature along with the statistical uncertainty to derive the uncertainty contribution due to the scalar and tensor shifts as 9×10^{-18}. The associated uncertainty of the trapping laser frequency is 3 MHz. Note that the first order Stark-shift cancelling frequency depends not only on the chosen m_F state but also on the angle between the polarization of the lattice light and the magnetic field; in our case these are collinear. When comparing to the values for the magic wavelength published in [7, 44] our value needs to be shifted by +286 MHz because of the tensor shift, and good agreement is found.

We now consider corrections and uncertainty contributions due to effects that are nonlinear in the lattice intensity. First, the hyperpolarizability correction at the operational lattice depth of 68 E_{rec} (thermally averaged) during the frequency measurement is -5×10^{-18} with an uncertainty of 2×10^{-18}, where we have allowed for 20% uncertainty in the intensity seen by the atoms and include the uncertainty of the published correction coefficient of 0.45 (10) $\mu\mathrm{Hz}/E_{\mathrm{rec}}^2$ [7]. Second, higher order interactions (magnetic dipole and electric quadrupole [47]) have not been observed, but an upper limit was derived in [44]. The shift is smaller than ± 0.31 $\mathrm{mHz}/\sqrt{E_{\mathrm{rec}}}$ leading to an uncertainty contribution of 6×10^{-18}.

Another uncertainty contribution related to the optical lattice arises from atoms tunnelling from site to site [48], thus introducing a first-order Doppler shift. In another picture, the periodicity of the trapping potential leads to energy bands that are not necessarily equally populated, which could cause line shifts on the order of the bandwidth. For a perfectly horizontal lattice with 80 E_{rec} depth, the width of the two lowest energy bands are 13 mHz and 826 mHz. According to [49], energy differences between sites lead to a suppression of the tunnelling, i.e., the bandwidths are reduced. The lattice is nearly horizontal with a small tilt of 2.7 mrad, leading to an energy difference of 2.4 Hz between two neighbouring sites due to gravity. The experimental observations of [49] support the reduction of the bandwidth by at least a factor of 50 for our parameters. We apply this and consider the population of the vibrational bands as derived from sideband spectra (see figure 2), i.e., fewer than 2% of the atoms are in the first axially excited band while no population remains in the second band due to the filtering, and we estimate a maximal fractional frequency shift due to tunnelling to be 1×10^{-18}.

3.3. Clock laser

Although low in intensity, the clock laser light may cause a frequency shift of the clock transition due to coupling to other states. With a measurement of the intensity and the sensitivity of $-13\,(2)\,\mathrm{Hz}\,(\mathrm{W\,cm^{-2}})^{-1}$ from [50] we determine that a light shift of less than 5×10^{-19} is caused by the clock laser, to which we assign an uncertainty of 1×10^{-18}.

A second uncertainty related to the clock laser needs to be considered: a drift of the clock laser reference cavity may lead to a systematic shift as the sides of the line are probed in the same order for each frequency correction. This effect is largely removed by drift-compensation with a linearly ramped AOM frequency. The residual systematic error is calculated to be 3×10^{-19} based on the update rate of the drift estimate (gain of $\beta = 0.02$ per correction) and the maximal observed change of the linear drift ($1.1 \times 10^{-7}\,\mathrm{Hz\,s^{-2}}$) according to equation (5) in [21].

3.4. Transfer of clock laser light and Doppler effect

The clock laser light is transferred via optical fibres both to a frequency comb and to the Sr atoms. Both transfers use single mode, polarization-maintaining fibres and optical path length stabilizations. The uncompensated optical path is kept below 0.5 m. While the path length stabilization for the link to the comb is active at all times, the stabilization of the path to the atoms is operated only during the interrogation pulses. The transient behaviour during switching was identified as possible error-source. We investigated this as described in [41] and obtain an uncertainty contribution of the optical path length stabilization of 8×10^{-19} under present experimental conditions[3]. Since the mirror producing the standing wave of the optical lattice is used as reference for the remote fibre end, first order Doppler shifts due to lattice vibrations or AOM chirps due to heating are removed. Second order Doppler shifts are not significant here.

The same AOM used for pulsing the clock laser and optical path length stabilization also provides the shift from the line centre to the desired m_F component and the chosen side of the probed line. The power of the diffracted light depends on the frequency of the AOM, which in principle leads to asymmetric excitation probabilities at the low and high frequency halfwidth

---

[3] We benefit from longer clock pulses compared to previous work due to a smaller clock laser instability.

points that would be incorrectly interpreted as line shifts. However, this effect is negligibly small.

3.5. Cold collisional shifts

Several atoms occupy each lattice site and collisions may shift the resonance frequency [18]. We have measured the density-dependent frequency shift by interleaving interrogations with few and many Sr atoms, which is realized by different loading times of the first stage MOT. The observed frequency shift is consistent with zero. A linear scaling (see e.g. [51]) to the atom number used in our frequency measurement results in an uncertainty of 5×10^{-18}. Typically the clock is operated with about 1500 atoms.

3.6. Collisions with background gas

We follow [52] to relate expected frequency shifts due to collisions with background gas atoms and molecules to observed trap lifetimes. We estimate the particle density for a number of gases (H, H_2, He and Xe) to reproduce our observed trap lifetime of 7 s (last term in equation (3) in [52]). We then determine the expected frequency shift using the long-range coefficients C_6 for both clock states[4]. The ratio of C_6 coefficients of the two clock states varies weakly between typical background gas species [53], and we finally assign a correction of $1.5\,(15) \times 10^{-18}$.

3.7. Line pulling

After the spin-polarization and purification steps, the population is almost entirely in the chosen m_F state, but residual populations in other m_F states may persist. Transitions driven from neighbouring m_F components will lead to a line pulling by creating an asymmetric background on the observed line. We derive experimentally an upper limit of 5% for atoms in other states, and with the known detuning of the π-transition of $m_F = \pm 7/2$, the line pulling effect is found to be less than 2×10^{-19}.

   If the polarization of the laser is not parallel to the quantization axis set by the magnetic field, i.e. due to birefringence of the viewports or a tilt of the polarization axis, another line pulling effect may occur: instead of a π-polarization coupling scheme with just the two $m_F = \pm 9/2$ levels, the admixing of sigma polarization couples to the $m_F = \pm 7/2$ state. In this Λ-scheme the π and σ-transitions are driven coherently, in which case an incoherent superposition of line profiles is not an adequate description. Instead, we numerically integrated the time-dependent Schrödinger equation of the three-level system and obtained an upper limit for the frequency shift of 2×10^{-19}, where we assumed a fractional power in the σ-polarization of less than 11%. This upper limit is derived from the minimal signal of a σ-transition that would have been visible on scans of the expected position of that transition. These two line pulling effects combined contribute an uncertainty of 3×10^{-19} fractional frequency shift.

3.8. Zeeman shifts

Stabilizing the clock laser to the average frequency of the two Zeeman components not only removes the linear Zeeman shift and the vector light shift (the magnetic field stability over

---

[4] The approximation using ΔC made in [52] was undone to account for differences of the long-range coefficients of typically 30%.

subsequent interrogation cycles is high enough) but also provides an estimate of the total magnetic field experienced by the atoms, including any stray fields provided that the lattice vector shift is small [44]. This enables a correction for the quadratic Zeeman shift, which is -3.2×10^{-17}. The associated uncertainty of 1.3×10^{-18} is mostly due to the uncertainty of the magnetic field as determined from the splitting of the clock transitions $m_F = -9/2$ and $+9/2$ of 240 Hz, while the correction coefficient contributes with negligible uncertainty (2×10^{-19}). During measurement of the magic wavelength, we measured the vector light shift to be smaller than 0.2 Hz, which can be neglected in the quadratic Zeeman shift correction.

3.9. dc electric fields

Residual static electric fields, e.g. from contact potentials, may be present that shift the frequency of the clock transition as observed in [54]. We have measured stray electric fields by applying additional electric fields and detecting the change of the transition frequency as a function of the applied field. The Stark shift is proportional to the square of the total electric field and hence a parabolic behaviour is observed. The projection of a residual electric field on the applied field is determined by the offset of the parabola from zero applied field strength. We have measured three projections of the stray field by applying moderate voltages to electrodes near the optical lattice. The known dc polarizability allows us to infer the applied field strength from the observed shift and applied voltage.

In order to derive the absolute value of the residual electric field from these three projections, the three angles between the applied fields must be determined. This is done by comparing the applied field strength with the observed projection of this field, which is seen in the parabola offset while generating a known electric field with one of the other two electrodes (much stronger than the residual field). With these measurements the residual electric field was found to be 15.8(22) V m^{-1}. The observed field is likely due to a voltage difference of about 0.7 V between the two coils providing the bias magnetic field, which is mostly caused by a protection diode between the coils.

During the frequency measurement, however, the electric field was larger because the magnetic field coils had not been operated near ground potential but rather at a potential of about 21 V, while the nearby capacitor used in [38] was grounded. With hindsight, we measured the frequency shift with an interleaved stabilization, alternating the voltage on the coils between 21 V and ground. The observed shift of -1.52×10^{-16} is consistent with the expected electric field strength and is included as a correction in the uncertainty budget. The associated uncertainty (3.3×10^{-17}) is mostly due to instabilities of the potential of the coils of ± 2 V. We now operate the experiment with the coils near ground potential to remove this considerable uncertainty.

4. Absolute frequency measurement

The frequency of the strontium lattice clock was measured against the two caesium fountain clocks CSF1 and CSF2 operated at PTB [34, 55–57], which are among the best primary frequency standards. During the measurement, an ytterbium ion clock based on the octupole transition $^2\mathrm{S}_{1/2}$ ($F = 0$) $- ^2\mathrm{F}_{7/2}$ ($F = 3$) of $^{171}\mathrm{Yb}^+$ [4, 58] was used as a flywheel oscillator, which allows us to bridge gaps in the operation of the Sr clock and extend the usable averaging time versus the Cs fountains. To improve the stability of CSF2 we utilized the Yb$^+$ clock laser to
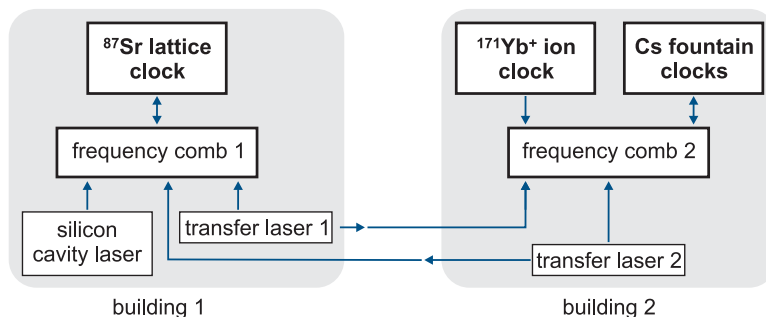
Figure 4. Overall experimental setup of the frequency measurement. Two frequency combs are employed to connect two optical clocks and the Cs fountain clocks as well as for the transfer of frequency stability. The connection between these combs, i.e., between two buildings separated by 300 m, is established by stabilized optical fibre links.

transfer its stability to the microwave regime with the help of a fs-laser frequency comb [8, 59, 60].

The overall setup of the frequency measurements is shown in figure 4. We employ two frequency combs, one in each building. Two ultrastable cw-laser at 871 nm and 1543 nm link these two combs. This twofold connection establishes a loop geometry that enables the characterization of this transfer scheme with respect to accuracy, stability, and reliability. Moreover, stabilized optical links between the buildings are preferable to traditional microwave links because they are less susceptible to thermally-driven phase shifts that caused a significant uncertainty contribution in our previous measurement [21].

Most of the optical paths of the measurement set-up are actively stabilized. The residual few meters of yet unstabilized optical path are passively shielded against environmental perturbations and their length variations influence the measurement. Based on a loop measurement with the two transfer lasers and the two combs, we derive an uncertainty contribution due to the frequency comparison in the optical regime of less than 1×10^{-18}. To ensure this accuracy, the synchronization of the dead-time free Π-counters in the two buildings is established via a pulse-per-second signal, and the propagation time ($<1\mu$s) is the only known source of a temporal offset between the gates of the counters at both frequency combs. Gate synchronization is important to ensure proper noise correlation and to avoid frequency offsets due to frequency drifts of the transfer lasers. To detect possible cycle slips in the phase tracking of the signals we split each beat signal and record it twice after independent filtering and phase tracking. A differential phase offset of 2π is taken as indication for a cycle slip and led to an exclusion of the data point.

The data analysis to derive the frequency of the strontium clock is performed in two steps:

- The frequency of the Yb$^+$ clock was measured relative to the Cs fountains for a total time of approximately 350 000 s between the 10 and 18 December 2012. This leads to statistical uncertainties of 2.5×10^{-16} and 2.0×10^{-16} due to the instabilities of the Cs fountains and the observed white-noise $1/\sqrt{\tau}$ dependence of the frequency measurement (see figure 3). The systematic uncertainties of the Cs fountains are 7.3×10^{-16} for CSF1 and 4.0×10^{-16} for CSF2. Averaging the two obtained frequency values leads to an uncertainty of 3.88×10^{-16}.

Table 2. Uncertainties of the absolute frequency measurement given in fractional frequencies.

Effect	Uncertainty (10^{-17})
Comparison Cs and Yb$^+$ including realization of the SI second	38.8
Statistics of Yb$^+$ and Sr comparison	1.3
Sr systematics	5.2
Transfer scheme	0.1
Gravitational red shift	0.07
Total	39

- In the same period, the frequency ratio of the strontium standard and the Yb$^+$ standard was measured for a total of approximately 165 000 s. We observe a clean $1/\sqrt{\tau}$ characteristic of the total Allan deviation in this comparison, leading to a statistical uncertainty of 1.3×10^{-17} for the comparison of the Yb$^+$ and the Sr clock.

Because both measurements show white frequency noise dependence, we can use the longer measurement time of the Yb$^+$ clock against the Cs fountain clocks to improve the statistical uncertainty of the Sr–Cs measurement, while not requiring a systematic frequency shift evaluation of the Yb$^+$ clock. This procedure leads to an absolute frequency measurement of the Sr clock transition with a relative frequency uncertainty of 3.9×10^{-16} (see table 2). We included the correction of the gravitational red shift due to the height difference between the Cs fountains and the Sr clock, which was determined in a levelling measurement with 6 mm uncertainty.

5. Results and discussion

We have measured the absolute frequency of the ^{87}Sr clock transition to be 429 228 004 229 873.13(17) Hz. This result agrees well with previous measurements and the recommended value by BIPM as shown in figure 5. In particular, we find excellent agreement between our result and the recent high-accuracy measurement from LNE-SYRTE [7], demonstrating one of the best levels of agreement between two independent measurements of the same physical quantity.

With proper grounding of the magnetic field coils, the dc Stark shift and its uncertainty is largely removed. In combination with the demonstrated uncertainty in the BBR shift correction due to reduced thermal load, the Sr frequency standard is now operated with a systematic uncertainty of 3×10^{-17}. Progress in reducing the BBR uncertainty further will likely require improved control over the thermal environment [24] or direct measurement of the radiation field [22]. If the lattice clock is operated at room temperature, the accuracy is currently limited by the knowledge of the atomic reaction to the BBR field, in particular the so-called dynamic contribution [28, 38], to an uncertainty of about 4×10^{-18}. Though this correction can in principle be quantified better by a measurement of dipole matrix elements as demonstrated for Yb [27], we believe that a reduction of the shift itself by lowering the environmental temperature is the more promising approach to reach uncertainties of 10^{-18} and below.
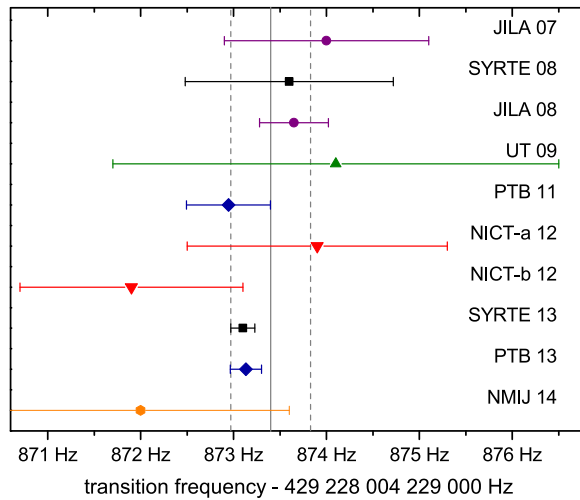
Figure 5. Comparison of measured absolute frequencies of the $5s^2\ ^1S_0 - 5s5p\ ^3P_0$ transition in ^{87}Sr. The frequencies are taken from these publications: JILA 07 [61], SYRTE 08 [62], JILA 08 [63], UT 09 [64], PTB 11 [21], NICT-a 12 [65], NICT-b 12 [66], SYRTE 13 [7] and NMIJ 14 [67] while PTB 13 is obtained in this work. The vertical line indicates the recent recommendation by the BIPM in 2013 [68] while the dashed lines show the assigned frequency uncertainty of 1×10^{-15}. The frequencies and uncertainties from data published before 2013 are not updated with improved knowledge on the blackbody correction coefficients [28, 38].

Any future design of our Sr standard aiming at a further reduction of the uncertainty should not only address the BBR shift but also orient the lattice along gravity [48]: given the current knowledge of the shift coefficients [44], higher order effects in the lattice light intensity will limit the total uncertainty at the 10^{-17} level in our apparatus because of the relatively deep trap needed to levitate the atoms against gravity in a horizontal lattice.

Direct comparisons of optical clocks already provide smaller relative uncertainties [1, 17, 19, 22] in the frequency ratio than can be achieved with absolute frequency measurements. Nonetheless, additional absolute frequency measurements such as the one described here are needed to provide a solid basis for a discussion of a re-definition of the SI second.

Acknowledgements

References

[1] Rosenband T *et al* 2008 Frequency ratio of Al$^+$ and Hg$^+$ single-ion optical clocks; metrology at the XVII decimal place *Science* **319** 1808–12

[2] Akatsuka T, Takamoto M and Katori H 2008 Optical lattice clocks with non-interacting bosons and fermions *Nat. Phys.* **4** 954–9

[3] Lemke N D, Ludlow A D, Barber Z W, Fortier T M, Diddams S A, Jiang Y, Jefferts S R, Heavner T P, Parker T E and Oates C W 2009 Spin-1/2 optical lattice clock *Phys. Rev. Lett.* **103** 063001

[4] Huntemann N, Okhapkin M, Lipphardt B, Weyers S, Tamm Chr and Peik E 2012 High-accuracy optical clock based on the octupole transition in ^{171}Yb$^+$ *Phys. Rev. Lett.* **108** 090801

[5] Madej A A, Dubé P, Zhu Z, Bernard J E and Gertsvolf M 2012 ^{88}Sr$^+$ 445-THz single ion reference at the 10^{-17} level via control and cancellation of systematic uncertainties and its measurement against the SI second *Phys. Rev. Lett.* **109** 203002

[6] McFerran J J, Yi L, Mejriand S, di Manno S, Zhang W, Guéna J, le Coq Y and Bize S 2012 Neutral atom frequency reference in the deep ultraviolet with fractional uncertainty $= 5.7 \times 10^{-15}$ *Phys. Rev. Lett.* **108** 183004

[7] Le Targat R *et al* 2013 Experimental realization of an optical second with strontium lattice clocks *Nat. Commun.* **4** 2109

[8] Tamm Chr, Huntemann N, Lipphardt B, Gerginov V, Nemitz N, Kazda M, Weyers S and Peik E 2014 A Cs-based optical frequency measurement using cross-linked optical and microwave oscillators *Phys. Rev.* A **89** 023820

[9] Bjerhammar A 1985 On a relativistic geodesy *Bull. Géodésique* **59** 207–20

[10] Schiller S *et al* 2009 Einstein gravity explorer—a medium-class fundamental physics mission *Exp. Astron.* **23** 573–610

[11] Chou C W, Hume D B, Rosenband T and Wineland D J 2010 Optical clocks and relativity *Science* **329** 1630–3

[12] Peik E, Lipphardt B, Schnatz H, Schneider T, Tamm Chr and Karshenboim S G 2004 Limit on the present temporal variation of the fine structure constant *Phys. Rev. Lett.* **93** 170801

[13] Fortier T M *et al* 2007 Precision atomic spectroscopy for improved limits on variation of the fine structure constant and local position invariance *Phys. Rev. Lett.* **98** 070801

[14] Blatt S *et al* 2008 New limits on coupling of fundamental constants to gravity using ^{87}Sr optical lattice clocks *Phys. Rev. Lett.* **100** 140801

[15] Peik E 2010 Fundamental constants and units and the search for temporal variations *Nucl. Phys.* B **203–204** 18–32

[16] Katori H, Takamoto M, Pal'chikov V G and Ovsiannikov V D 2003 Ultrastable optical clock with neutral atoms in an engineered light shift trap *Phys. Rev. Lett.* **91** 173005

[17] Chou C W, Hume D B, Koelemeij J C J, Wineland D J and Rosenband T 2010 Frequency comparison of two high-accuracy Al$^+$ optical clocks *Phys. Rev. Lett.* **104** 070802

[18] Nicholson T L, Martin M J, Williams J R, Bloom B J, Bishof M, Swallows M D, Campbell S L and Ye J 2012 Comparison of two independent Sr optical clocks with 1×10^{-17} stability at 10^3 s *Phys. Rev. Lett.* **109** 230801

[19] Hinkley N, Sherman J A, Phillips N B, Schioppo M, Lemke N D, Beloy K, Pizzocaro M, Oates C W and Ludlow A D 2013 An atomic clock with 10^{-18} instability *Science* **341** 1215–8

[20] Ludlow A D *et al* 2008 Sr lattice clock at 1×10^{-16} fractional uncertainty by remote optical evaluation with a Ca clock *Science* **319** 1805–8

[21] Falke St, Schnatz H, Vellore Winfred J S R, Middelmann Th, Vogt St, Weyers S, Lipphardt B, Grosche G, Riehle F, Sterr U and Lisdat Ch 2011 The ^{87}Sr optical frequency standard at PTB *Metrologia* **48** 399–407

[22] Bloom B J, Nicholson T L, Williams J R, Campbell S L, Bishof M, Zhang X, Zhang W, Bromley S L and Ye J 2014 An optical lattice clock with accuracy and stability at the 10^{-18} level *Nature* **506** 71–5

[23] Porsev S G and Derevianko A 2006 Multipolar theory of blackbody radiation shift of atomic energy levels and its implications for optical lattice clocks *Phys. Rev.* A **74** 020502

[24] Middelmann Th, Lisdat Ch, Falke St, Vellore Winfred J S R, Riehle F and Sterr U 2011 Tackling the blackbody shift in a strontium optical lattice clock *IEEE Trans. Instrum. Meas.* **60** 2550–7

[25] Sherman J A, Lemke N D, Hinkley N, Pizzocaro M, Fox R W, Ludlow A D and Oates C W 2012 High accuracy measure of atomic polarizability in an optical lattice clock *Phys. Rev. Lett.* **108** 153002

[26] Safronova M S, Porsev S G and Clark C W 2012 Ytterbium in quantum gases and atomic clocks: van der Waals interactions and blackbody shifts *Phys. Rev. Lett.* **109** 230802

[27] Beloy K, Sherman J A, Lemke N D, Hinkley N, Oates C W and Ludlow A D 2012 Determination of the $5d6s$ $^{3}D_{1}$ state lifetime and blackbody-radiation clock shift in Yb *Phys. Rev.* A **86** 051404

[28] Safronova M S, Porsev S G, Safronova U I, Kozlov M G and Clark C W 2013 Blackbody radiation shift in the Sr optical atomic clock *Phys. Rev.* A **87** 012509

[29] Jiang Y Y, Ludlow A D, Lemke N D, Fox R W, Sherman J A, Ma L-S and Oates C W 2011 Making optical atomic clocks more stable with 10^{-16} level laser stabilization *Nat. Photon.* **5** 158–61

[30] Kessler T, Hagemann C, Grebing C, Legero T, Sterr U, Riehle F, Martin M J, Chen L and Ye J 2012 A sub-40 mHz linewidth laser based on a silicon single-crystal optical cavity *Nat. Photon.* **6** 687–92

[31] Hagemann C, Grebing C, Kessler T, Falke S, Lemke N, Lisdat C, Schnatz H, Riehle F and Sterr U 2013 Providing 10^{-16} short-term stability of a 1.5 μm laser to optical clocks *IEEE Trans. Instrum. Meas.* **62** 1556–62

[32] Heavner T P, Jefferts S R, Donley E A, Shirley J H and Parker T E 2005 NIST-F1: recent improvements and accuracy evaluations *Metrologia* **42** 411–22

[33] Li R, Gibble K and Szymaniec K 2011 Improved accuracy of the NPL-CsF2 primary frequency standard: evaluation of distributed cavity phase and microwave lensing frequency shifts *Metrologia* **48** 283–9

[34] Weyers S, Gerginov V, Nemitz N, Li R and Gibble K 2011 Distributed cavity phase frequency shifts of the caesium fountain PTB-CSF2 *Metrologia* **49** 82–87

[35] Guéna J *et al* 2012 Progress in atomic fountains at LNE-SYRTE *IEEE Trans. Ultrason. Ferroelectr. Frequation Control* **59** 391–410

[36] BIPM 1988–2014 *CircularT* monthly www.bipm.org/jsp/en/TimeFtp.jsp.

[37] Lisdat Ch, Vellore Winfred J S R, Middelmann T, Riehle F and Sterr U 2009 Collisional losses, decoherence, and frequency shifts in optical lattice clocks with bosons *Phys. Rev. Lett.* **103** 090801

[38] Middelmann T, Falke S, Lisdat C and Sterr U 2012 High accuracy correction of blackbody radiation shift in an optical lattice clock *Phys. Rev. Lett.* **109** 263004

[39] Mukaiyama T, Katori H, Ido T, Li Y and Kuwata-Gonokami M 2003 Recoil-limited laser cooling of Sr atoms near the Fermi temperature *Phys. Rev. Lett.* **90** 113002

[40] Blatt S, Thomsen J W, Campbell G K, Ludlow A D, Swallows M D, Martin M J, Boyd M M and Ye J 2009 Rabi spectroscopy and excitation inhomogeneity in a one-dimensional optical lattice clock *Phys. Rev.* A **80** 052703

[41] Falke S, Misera M, Sterr U and Lisdat C 2012 Delivering pulsed and phase stable light to atoms of an optical clock *Appl. Phys.* B **107** 301–11

[42] BIPM 2008 *JCGM 100:2008. Evaluation of Measurement Data—Guide to the Expression of Uncertainty in Measurement* www.bipm.org/utils/common/documents/jcgm/JCGM_100_2008_E.pdf

[43] Wieting T J and DeRosa J L 1979 Effects of surface condition on the infrared absorptivity of 304 stainless steel *J. Appl. Phys.* **50** 1071

[44] Westergaard P G, Lodewyck J, Lorini L, Lecallier A, Burt E A, Zawada M, Millo J and Lemonde P 2011 Lattice-induced frequency shifts in Sr optical lattice clocks at the 10^{-17} level *Phys. Rev. Lett.* **106** 210801

[45] Degenhardt C *et al* 2005 Calcium optical frequency standard with ultracold atoms: approaching 10^{-15} relative uncertainty *Phys. Rev. A* **72** 062111

[46] Howe D A 1999 The total deviation approach to long-term characterization of frequency stability *IEEE Trans. Ultrason. Ferroelectr. Freq. Control* **47** 1102–10

[47] Taichenachev A V, Yudin V I, Ovsiannikov V D, Pal'chikov V G and Oates C W 2008 Frequency shifts in an optical lattice clock due to magnetic-dipole and electric-quadrupole transitions *Phys. Rev. Lett.* **101** 193601

[48] Lemonde P and Wolf P 2005 Optical lattice clock with atoms confined in a shallow trap *Phys. Rev. A* **72** 033409

[49] Sias C, Lignier H, Singh Y P, Zenesini A, Ciampini D, Morsch O and Arimondo E 2008 Observation of photon-assisted tunneling in optical lattices *Phys. Rev. Lett.* **100** 040404

[50] Baillard X, Fouché M, Targat R L, Westergaard P G, Lecallier A, Coq Y L, Rovera G D, Bize S and Lemonde P 2007 Accuracy evaluation of an optical lattice clock with bosonic atoms *Opt. Lett.* **32** 1812–4

[51] Sortais Y, Bize S, Nicolas C, Clairon A, Salomon C and Williams C 2000 Cold collision frequency shifts in a ^{87}Rb atomic fountain *Phys. Rev. Lett.* **85** 3117–20

[52] Gibble K 2013 Scattering of cold atom coherences by hot atoms: frequency shifts from background gas collisions *Phys. Rev. Lett.* **110** 180802

[53] Mitroy J and Zhang J Y 2010 Dispersion and polarization interactions of the strontium atom *Mol. Phys.* **108** 1999–2006

[54] Lodewyck J, Zawada M, Lorini1 L, Gurov M and Lemonde P 2012 Observation and cancellation of a perturbing dc Stark shift in strontium optical lattice clocks *IEEE Trans. Ultrason. Ferroelectr. Frequation Control* **59** 411

[55] Weyers S, Hübner U, Schröder R, Tamm Chr and Bauch A 2001 Uncertainty evaluation of the atomic caesium fountain CSF1 of the PTB *Metrologia* **38** 343–52

[56] Weyers S, Bauch A, Schröder R and Tamm C 2001 The atomic caesium fountain CSF1 of PTB *Proc. 6th Symp. on Frequency Standards and Metrology 2001* ed P Gill (Singapore: World Scientific) p 64

[57] Gerginov V, Nemitz N, Weyers S, Schröder R, Griebsch R D and Wynands R 2010 Uncertainty evaluation of the caesium fountain clock PTB-CSF2 *Metrologia* **47** 65–79

[58] Huntemann N, Lipphardt B, Okhapkin M, Tamm C, Peik E, Taichenachev A V and Yudin V I 2012 A generalized Ramsey excitation scheme with suppressed light shift *Phys. Rev. Lett.* **109** 213002

[59] Lipphardt B, Grosche G, Sterr U, Tamm C, Weyers S and Schnatz H 2009 The stability of an optical clock laser transferred to the interrogation oscillator for a Cs fountain *IEEE Trans. Instrum. Meas.* **58** 1258–62

[60] Weyers S, Lipphardt B and Schnatz H 2009 Reaching the quantum limit in a fountain clock using a microwave oscillator phase locked to an ultrastable laser *Phys. Rev. A* **79** 031803

[61] Boyd M M, Ludlow A D, Blatt S, Foreman S M, Ido T, Zelevinsky T and Ye J 2007 ^{87}Sr lattice clock with inaccuracy below 10^{-15} *Phys. Rev. Lett.* **98** 083002

[62] Baillard X *et al* 2008 An optical lattice clock with spin-polarized ^{87}Sr atoms *Eur. Phys. J. D* **48** 11–17

[63] Campbell G K *et al* 2008 The absolute frequency of the ^{87}Sr optical clock transition *Metrologia* **45** 539–48

[64] Hong F-L *et al* 2009 Measuring the frequency of a Sr optical lattice clock using a 120 km coherent optical transfer *Opt. Lett.* **34** 692–4

[65] Yamaguchi A, Shiga N, Nagano S, Li Y, Ishijima H, Hachisu H, Kumagai M and Ido T 2012 Stability transfer between two clock lasers operating at different wavelengths for absolute frequency measurement of clock transition in ^{87}Sr *Appl. Phys. Express* **5** 022701

[66] Matsubara K, Hachisu H, Li Y, Nagano S, Locke C, Nohgami A, Kajita M, Hayasaka K, Ido T and Hosokawa M 2012 Direct comparison of a Ca$^+$ single-ion clock against a Sr lattice clock to verify the absolute frequency measurement *Opt. Express* **20** 22034

[67] Akamatsu D, Inaba H, Hosaka K, Yasuda M, Onae A, Suzuyama T, Amemiya M and Hong F-L 2014 Spectroscopy and frequency measurement of the ^{87}Sr clock transition by laser linewidth transfer using an optical frequency comb *Appl. Phys. Express* **7** 012401

[68] Bureau International des Poids et Mesures (BIPM) 2013 *Report of the* 101th *Meeting of the Comité International des Poids et Mesures (CIPM)* (Paris: BIPM)